Factors influencing the martensitic transformation in $Ni_{50}Mn_{35}Sn_{15}$: an EXAFS study

2008 J. Phys.: Condens. Matter 20 015219

(http://iopscience.iop.org/0953-8984/20/1/015219)

J. Phys.: Condens. Matter **20** (2008) 015219 (8pp) doi:10.1088/0953-8984/20/01/015219

Factors influencing the martensitic transformation in $Ni_{50}Mn_{35}Sn_{15}$: an EXAFS study

P A Bhobe, K R Priolkar[1] and P R Sarode

Department of Physics, Goa University, Goa 403 206, India

E-mail: krp@unigoa.ac.in

Received 18 September 2007, in final form 10 November 2007
Published 7 December 2007
Online at stacks.iop.org/JPhysCM/20/015219

Abstract

Extended x-ray absorption fine-structure (EXAFS) measurements have been carried out on $Ni_{50}Mn_{35}Sn_{15}$ in the austenitic and martensitic phases. The temperatures associated with structural and magnetic phase transformations are obtained from magnetization measurements. The system orders ferromagnetically below 319 K while the structural phase transition occurs at $T_M \sim 200$ K. EXAFS measurements have been carried out at Mn and Ni K-edges and changes associated with respect to the local structure of these absorbing atoms are compared. Significant changes in the nearest neighbour interactions are seen as the system transits to the low temperature martensitic phase. EXAFS provides evidence for local structural distortion even in the cubic phase that is not seen from the x-ray diffraction studies. The results obtained are understood in terms of changing hybridization between the constituent atoms that influence the electronic structure at the Fermi level, associated with the austenitic to martensitic transition.

(Some figures in this article are in colour only in the electronic version)

1. Introduction

Martensitic transformations and their pairing with ferromagnetism have been a central subject for investigations in recent years. In particular, some intermetallics show simultaneous occurrence of martensitic and magnetic transitions, suggesting the possibility of controlling the structural transformation by magnetic field which could be exploited for practical applications. Such multifunctional materials are classified under the rapidly growing technological field of ferromagnetic shape memory alloys (FSMA). Among the variety of FSMA, Ni–Mn–Ga alloys are a recently synthesized class of alloys that have been studied extensively and hence serve as a reference in the development of new systems [1–3]. The stoichiometric Ni_2MnGa undergoes martensitic transition around 220 K from a $L2_1$ cubic phase to a low symmetry modulated structure, while the ferromagnetic transition takes place at 370 K [4]. An interesting aspect of Ni–Mn–Ga alloys is the isothermal giant entropy change obtained when structural and magnetic transition temperatures nearly coincide, leading to a development of new materials exhibiting the magnetocaloric effect [5].

[1] Author to whom any correspondence should be addressed.

The latest candidates in the field of FSMA have been alloys with composition $Ni_{50}Mn_{50-x}Z_x$ with Z = In, Sn, Sb [6]. Of particular interest is $Ni_{50}Mn_{50-x}Sn_x$ with $0.13 \leqslant x \leqslant 0.15$ for which an inverse magnetocaloric effect is observed that is nearly three times larger in comparison to those for other alloys [7]. This system orders ferromagnetically at a Curie temperature $T_C \sim 319$ K while martensitic transition occurs at temperature, $T_M \sim 200$ K [6]. Neutron diffraction experiments on $Ni_{50}Mn_{36}Sn_{14}$ show that the cubic $L2_1$ structure in the austenitic phase transforms to the orthorhombic $4O$ structure with *Pmma* space group in the martensitic phase [8]. Studies show that despite structural similarity with Ni_2MnZ alloys, strong differences in the underlying martensitic and magnetic properties are seen in $Ni_{50}Mn_{50-x}Sn_x$ [9, 10]. For example, while the martensitic transition is absent in the stoichiometric Ni_2MnSn, these Mn rich alloys exhibit martensitic transition over a wide range of temperatures [6]. Further, the magnetic moment of $Ni_{50}Mn_{36}Sn_{14}$ in the martensitic phase is smaller by about 50% than that in the cubic phase [10]. Even in the $L2_1$ phase, the Mn moments are significantly smaller than those reported for the stoichiometric Ni_2MnZ alloys [11, 8]. It is conjectured that apart from the ferromagnetic order, some

antiparallel alignment of the excess Mn moments could exist in $Ni_{50}Mn_{50-x}Sn_x$ [9, 8]. Thus an understanding of the local structure in the martensitic and austenitic phases is vital in establishing a complete picture of the transformation mechanics. Therefore, we have carried out *extended x-ray absorption fine structure* (EXAFS) measurements at Mn and Ni K-edges in the austenitic and martensitic phases of $Ni_{50}Mn_{35}Sn_{15}$.

2. Experimental details

A homogeneous bead of $Ni_{50}Mn_{35}Sn_{15}$ was prepared by repeated melting of the appropriate quantities of the constituent elements of 4N purity under argon atmosphere in an arc furnace. The sample bead so obtained was sealed in an evacuated quartz ampoule and annealed at 800 K for 48 h followed by quenching in cold water. Energy dispersive x-ray analysis that gave the elemental content as: Ni = 50.4, Mn = 34.6 and Sn = 15.0 confirmed the composition of the sample to be close to nominal. The sample bead was cut and thoroughly ground to a very fine powder for x-ray diffraction (XRD) and EXAFS measurements, while a small piece of the same bead was used for magnetization study. The room temperature crystal structure was determined by XRD recorded on a Rigaku D-MAX IIC diffractometer with Cu Kα radiation. The magnetization measurements were carried out on a Vibrating Sample Magnetometer in the low field value (50 Oe) and in the temperature range 50–350 K. EXAFS at Ni and Mn K-edges were recorded at room temperature and liquid nitrogen temperature in the transmission mode on the EXAFS-1 beamline at ELETTRA synchrotron source using Si(111) as monochromator. For this, the powder of $Ni_{50}Mn_{35}Sn_{15}$ was coated on Scotch-tape strips. These sample coated strips were adjusted in number such that the absorption edge jump gave $\Delta\mu x \leqslant 1$. The incident and transmitted photon energies were simultaneously recorded using gas-ionization chambers as detectors. Measurements were carried out from 300 eV below the edge energy to 1000 eV above it with a 5 eV step in the pre-edge region and 2.5 eV step in the EXAFS region. At each edge, three scans were collected. Data analysis was carried out using IFEFFIT [12] in ATHENA and ARTEMIS programs [13]. Here theoretical fitting standards were computed with ATOMS and FEFF6 programs [14, 15]. The data in the k range of (2–12) $Å^{-1}$ was used for analysis. For x-ray absorption near edge structure (XANES), the data were collected from 300 eV below the edge energy to 100 eV above the edge in steps of 5 eV from −300 to −50 eV; 0.2 eV from −50 to +50 eV and 1 eV for the rest of the spectra. Normalization was done by first subtracting the Victoreen instrument background obtained from fitting the pre-edge region (−200 to −50 eV) from all of the raw spectra and then dividing them by respective average absorption coefficients obtained for the spectral region +50 to +90 eV.

3. Results

Rietveld refinement of the room temperature XRD data confirms that the sample is highly ordered in the Heusler $L2_1$ structure with $Fm\bar{3}m$ space group and lattice parameters of

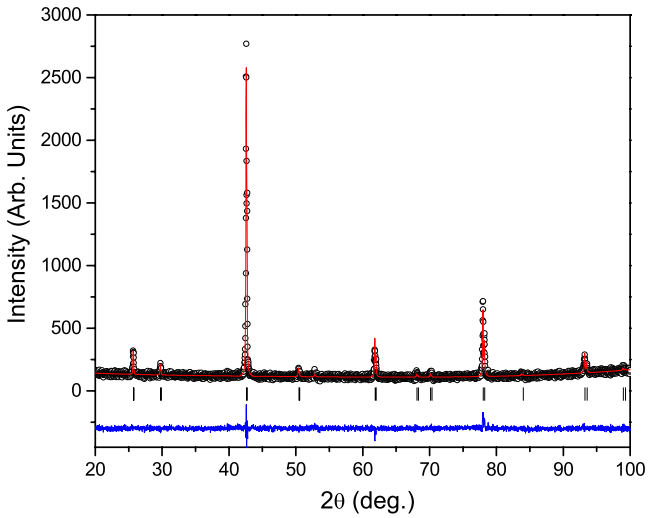

Figure 1. The x-ray powder diffraction pattern of $Ni_{50}Mn_{35}Sn_{15}$ at room temperature. The open circles show the observed counts and the continuous line passing through these counts is the calculated profile. The difference between the observed and calculated patterns is shown as a continuous line at the bottom of the two profiles. The calculated positions of the reflections are shown as vertical bars.

5.9941 ± 0.0003 Å. The observed and calculated diffraction patterns together with the difference pattern are shown in figure 1. In the stoichiometric Heusler composition X_2YZ, $Ni_{50}Mn_{35}Sn_{15}$ can be described as X = Ni occupying the $(\frac{1}{4}\frac{1}{4}\frac{1}{4})$ site, Y = Mn occupying the (000) site and Z = (60% Sn + 40% Mn) occupying the $(\frac{1}{2}\frac{1}{2}\frac{1}{2})$ site. To distinguish between the Mn occupying the (0, 0, 0) position and the excess Mn that occupies the Z sites, they will henceforth be referred to as Y-Mn and Z-Mn respectively.

Magnetization was determined in a field of 50 Oe over the temperature range 50–350 K. Initially, the sample was cooled from room temperature to 50 K in the absence of magnetic field. An external field of 50 Oe was applied and magnetization was recorded with increasing temperature up to 350 K (referred as zero field cooled, ZFC). The measurements were made as the sample was subsequently cooled to 50 K without disturbing the magnetic field (field cooled, FC) and finally the sample was field-heated (FH) up to 350 K. The ferromagnetic ordering sets in at the Curie temperature T_C = 319 K. As the temperature is lowered, magnetization remains essentially constant until 200 K where an abrupt fall in M is observed. This behaviour corroborates with that reported for the martensitic phase transition by [6, 8, 9] and [16] in Ni–Mn–Sn alloys. The ZFC, FC and FH magnetization curves are shown in figure 2. The martensitic start (M_s = 182.7 K), martensitic finish (M_f = 164.3 K), reverse martensitic or austenitic start (A_s = 176.2 K) and austenitic finish (A_f = 195.6 K) temperatures are identified and the thermal hysteresis is found to be ∼12 K. The hysteresis in the FC and FH curves is attributed to the structural transition while the splitting in the ZFC and FC curves just below T_C has been associated with competing magnetic interactions speculated in this system [9]. The presence of Z-Mn in the system gives rise to additional Mn–Mn interactions with antiparallel alignment of moments

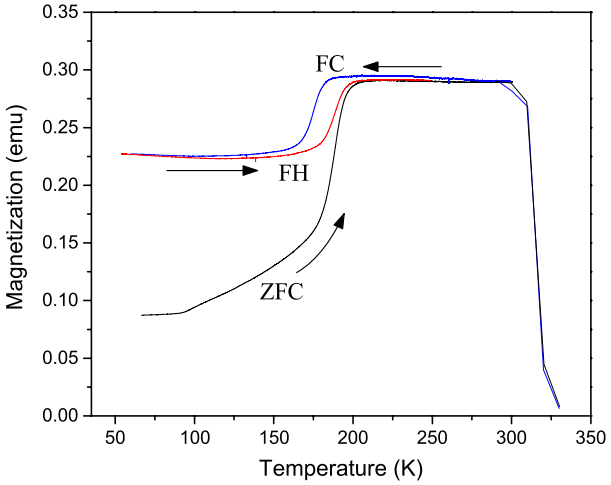

Figure 2. Temperature dependence of magnetization of $Ni_{50}Mn_{35}Sn_{15}$ measured in an applied field of 50 Oe between 50 and 350 K. Measurements were carried out while heating (ZFC), cooling (FC) and re-heating (FH) the sample as indicated by the arrows. The structural and magnetic transition temperatures were determined from the differentials of magnetization with respect to temperature for FC and FH curves.

that is responsible for the lower magnetic moments in the austenitic as well as martensitic phases.

The k-weighted $\chi(k)$ spectra at Mn and Ni K-edges at room temperature (RT) and liquid nitrogen temperature (LT) are shown in figure 3. It can be seen that there are distinct differences in the RT and LT spectra, especially in the k range of 4–7 $Å^{-1}$ which can be ascribed to martensitic transformation of the sample. With the knowledge of crystal structure from XRD, a cubic $L2_1$ model with $a = 5.994$ Å was adapted for the analysis of RT data. Here, the most relevant contribution to EXAFS in the R-range 1.0–5.0 Å, comes from near neighbour interactions that comprise of four single scattering (SS) paths and one linear multiple scattering (MS) path along the body diagonal of the initial cubic cell, as shown schematically in figure 4(a). As per the $L2_1$ model, the second SS path is entirely due to scattering from Z atoms. Due to the presence of excess Mn in $Ni_{50}Mn_{35}Sn_{15}$, the Z site is occupied by two different type of atoms, Sn and Mn. In order to incorporate the contribution from both these atoms occupying the Z site, two fitting standards were calculated in the FEFF input file. The first fitting standard was calculated with Sn atoms alone occupying the Z site, while in the second, only Mn atoms were considered to be entirely occupying the Z site. Both these fitting standards were then introduced in the model with respective path coordination numbers changed as per the actual composition ratio (Sn:Mn = 60:40). The structure being cubic at room temperature, the correction to the path lengths δR_j was refined with a constraint, $\delta R_j = \delta r_1 \times [(R_{\text{eff}})_j / R_{\text{nn1}}]$ where R_{nn1} is the nearest neighbour distance, kept fixed to 2.5955 Å (calculated from the lattice constant), $(R_{\text{eff}})_j$ is the calculated bond length for each coordination shell j obtained from FEFF and δr_1 is the change in first neighbour distance. By varying δr_1 alone, a correction is applied to all the bond lengths simultaneously. The thermal mean-square variations in the bond lengths, σ^2 were varied independently for each path considered in the fit. Such an approach to data analysis has been successfully used for the EXAFS of $Ni_{2+x}Mn_{1-x}Ga$ alloys [17]. The present fit gives the first neighbour, Mn–Ni distance equal to 2.549 Å which is much shorter than 2.5955 Å, the value calculated from the lattice constant. This points towards some disorder at the local level in the cubic structure. However, no structural disorder is seen either in the XRD profile (refer figure 1) or in the neutron diffraction study by Brown *et al* [8] on the $Ni_{50}Mn_{36}Sn_{14}$ system.

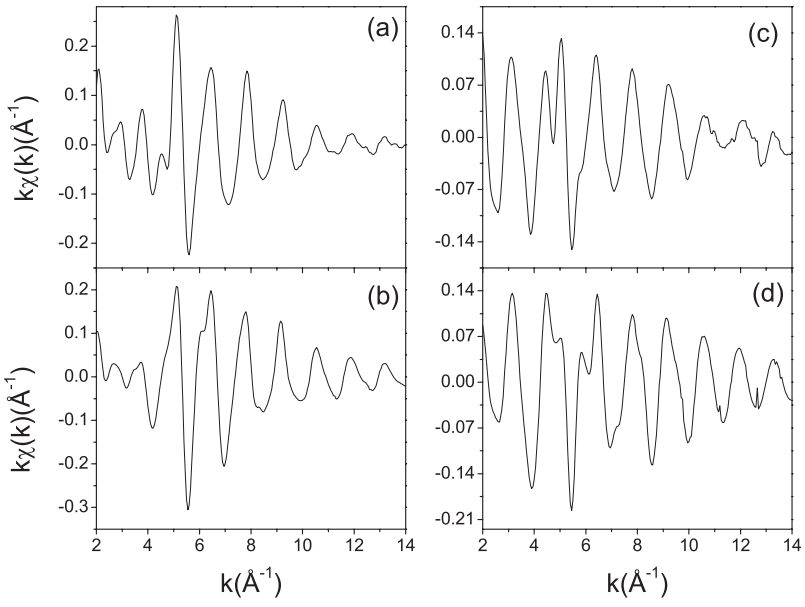

Figure 3. The k-weighted $\chi(k)$ spectra of $Ni_{50}Mn_{35}Sn_{15}$ recorded at (a) room temperature Mn K-edge, (b) low temperature Mn K-edge, (c) room temperature Ni K-edge and (d) low temperature Ni K-edge. These data were Fourier transformed in the range (2–12) ($Å^{-1}$) for analysis.

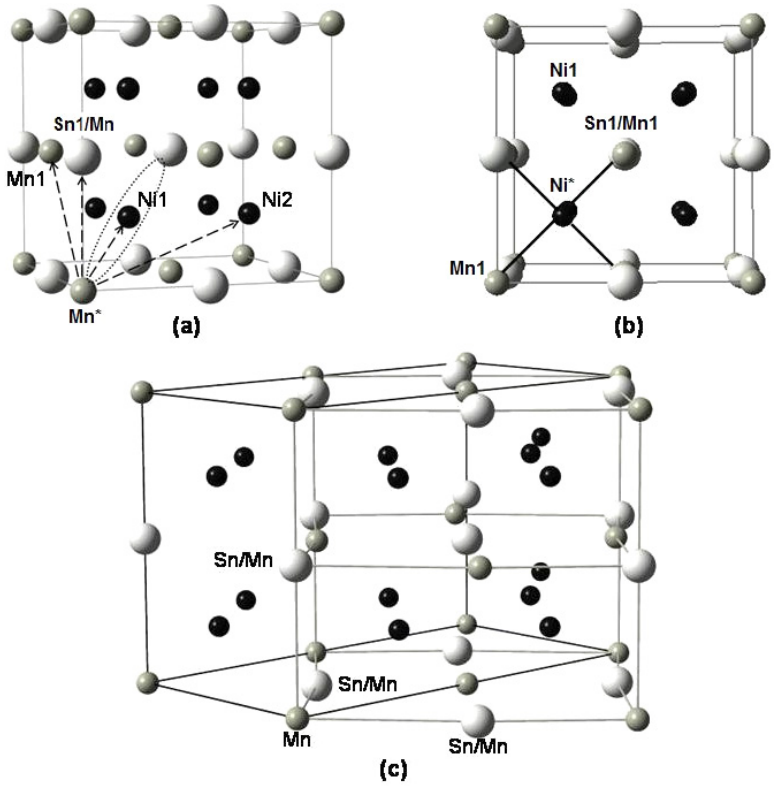

Figure 4. The crystal structure of $Ni_{50}Mn_{35}Sn_{15}$ based on which the EXAFS have been modelled. (a) The $L2_1$ cubic phase shows the absorbing atom (indicated with $*$) and the relevant backscatters. The arrows indicate different SS paths while the dotted loop shows the MS path. (b) The plane of atoms in the cubic crystal represents the fact that Mn(Y site) and Sn/Mn(Z site) are equidistant from Ni. (c) The *Pmma* crystal structure in the martensitic phase wherein the $L2_1$ type atomic arrangement is visualized.

In the case of Ni K-edge EXAFS the fitting was carried out in the R-range 1.0–3.0 Å. The peak in this range of the spectra comprises of Ni–Mn, Ni–Sn and Ni–Ni single scattering paths. An analysis similar to that of Mn EXAFS, with constrained refinement of δR, was carried out. However, this did not result in a good fit. To overcome this situation, δrs for each of the three scattering paths were varied independently. As can be seen in figure 5, a good fit was obtained for the values listed in table 1. It is interesting to note that the Ni–Mn bond length is distinctly shorter than the Ni–Sn bond length. Further, the Ni–Sn and Ni–Ni bond lengths match closely with the values calculated from the room temperature XRD data.

In the cubic $L2_1$ structure, the X site(Ni) is surrounded by four Y site(Mn) and four Z site(Sn) atoms at exactly equal distance (figure 4(b)). Therefore a difference in the Ni–Mn and Ni–Sn bond lengths obtained from EXAFS analysis conclusively points towards a local structural disorder in the cubic phase. The Ni–Mn bond length is actually the weighted average distance of Ni from the Y-Mn and the Z-Mn. Ideally, for a $L2_1$ structure, both these contributions should have been identical and equal to the Ni–Sn bond distance. A possible explanation for the discrepancy in the Ni–Mn bond length can be that the two contributions (Ni–[Y-Mn] and Ni–[Z-Mn]) are not equal. That is, there is a slight difference in the bond distance of Y-Mn and the Z-Mn from Ni, giving an average Ni–Mn distance shorter than expected. In order to confirm this, Mn EXAFS data were fitted again with the δrs and σ^2 varied independently for each path. The resulting fit was excellent as can be seen from figure 6 and the final fitted parameters are listed in table 1. It can be seen that the distances

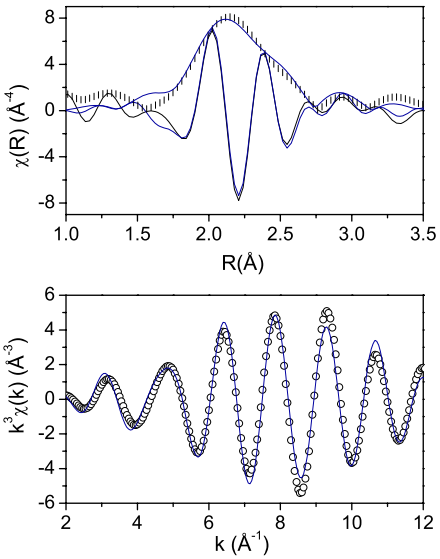

Figure 5. Magnitude and real component of FT of EXAFS spectra in R space (top panel) and the real component of FT in the back transformed k space (bottom panel) for the Ni K-edge in $Ni_{50}Mn_{35}Sn_{15}$ obtained at room temperature. The fitting to the data is shown as a solid line.

Table 1. Parameters for the cubic and martensitic phases of $Ni_{50}Mn_{35}Sn_{15}$ determined from the analysis of Mn and Ni K-edge EXAFS recorded at room temperature (RT) and low temperature (LT). The calculated distances for the $L2_1$ cell (with $a = 5.994$ Å) are also mentioned. R refers to the bond length and σ^2 is the thermal mean square variation in the bond length. The analyses were carried out in the k range: (2–12) $Å^{-1}$ with k-weight: 3 and R range: (1–5) Å for Mn edge and (1–3) Å for Ni edge. Figures in parentheses indicate uncertainty in the last digit.

RT—cubic phase				LT—Martensitic phase		
Atom and coord. No.	$L2_1$ model R_{calc} (Å)	R (Å)	σ^2 ($Å^2$)	Atom and coord. No.	R (Å)	σ^2 ($Å^2$)
			Mn K-edge			
Ni1 × 8	2.595	2.549(6)	0.0127(7)	Ni1 × 8	2.568(1)	0.0077(1)
Sn1 × 3.6	2.997	2.95(2)	0.012(2)	Sn1 × 3.6	2.873(3)	0.0069(3)
Mn × 2.4	2.997	2.93(1)	0.008(1)	Mn × 2.4	2.877(4)	0.0095(5)
Mn1 × 12	4.239	4.21(2)	0.021(3)	Mn1 × 8	4.17(2)	0.023(3)
Ni2 × 24	4.970	4.95(2)	0.019(2)	Mn2 × 4	4.291(9)	0.008(1)
MS[a] × 16	5.191	5.098(3)	0.014(1)	Ni2 × 16	4.753(6)	0.0088(7)
				Ni3 × 8	4.940(3)	0.0086(3)
			Ni K-edge			
Mn1 × 5.6	2.595	2.550(7)	0.0132(9)	Mn1 × 5.6	2.569(2)	0.0092(2)
Sn1 × 2.4	2.595	2.601(7)	0.0072(6)	Sn1 × 2.4	2.607(1)	0.0035(1)
Ni1 × 6	2.997	2.98(3)	0.026(5)	Ni1 × 2	2.83(1)	0.016(2)
				Ni2 × 4	3.15(3)	0.027(5)

[a] Mn → Sn3 → Ni1 → Mn.

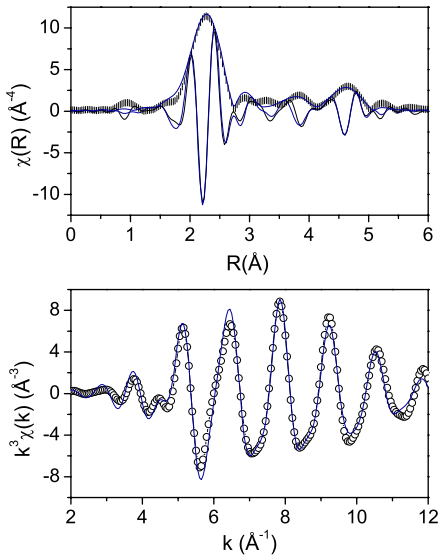

Figure 6. Magnitude and real component of FT of EXAFS spectra in R space and real component of FT in the back transformed k space for Mn K-edge in $Ni_{50}Mn_{35}Sn_{15}$ obtained at room temperature. The fittings to the data are shown as solid lines.

obtained from Mn EXAFS analysis are indeed lower than the distances calculated from the diffraction data, confirming the local disorder in cubic structure.

As the martensitic transformation is in the vicinity of 200 K, EXAFS measured at liquid nitrogen temperature (∼77 K) contains no residual cubic component and was used to determine the local structure of the martensitic phase. Neutron diffraction studies by Brown *et al* [8] show that $Ni_{50}Mn_{36}Sn_{14}$ transforms to a 4*O* orthorhombic structure with *Pmma* space group in the martensitic phase. Figure 4(c) represents the *Pmma* crystal structure within which a $L2_1$ type sub-cell can be visualized. On comparing this structure with the different scattering paths shown in the $L2_1$ phase of figure 4(a), it can be clearly understood that with Mn as the central atom, several closely spaced Mn–Ni, Mn–Sn and Mn–Mn bonds are obtained. EXAFS is generally insensitive in resolving such closely spaced scattering paths. Hence, to model the low temperature EXAFS data, these closely spaced scattering paths were grouped into one or two correlations, as shown in figure 4. The coordination number for the Mn-[Sn/Mn] paths was maintained in accordance with the composition ratio of Mn and Sn. The δrs and σ^2s for each of the scattering paths were varied independently without any constraint. Similar fitting procedure was also followed in the case of Ni EXAFS. The values given in table 1 were found to give a good fit to the experimental spectra, as can be seen from figures 7 and 8. While an increase of 0.02 Å is seen in the Mn–Ni bond distance, the first Mn–Sn and Mn–Mn distances shorten to 2.87 Å from those obtained in the austenitic phase. Likewise, the parameters obtained from the analysis of low temperature Ni EXAFS (refer table 1) show that the Ni–Mn distance indeed increases and is in good agreement with the value obtained from Mn EXAFS. The most significant observation here is that the Ni–Sn distance remains unchanged from its room temperature value. This implies that the low temperature modulated structure is due to an unequal movement of constituent atoms with Mn moving with the largest amplitude.

4. Discussion

EXAFS measurements in the cubic and martensitic phases of $Ni_{50}Mn_{35}Sn_{15}$ bring out an important observation that influences the martensitic transition in this system. Essentially, the present system belongs to the Ni–Mn based ternary

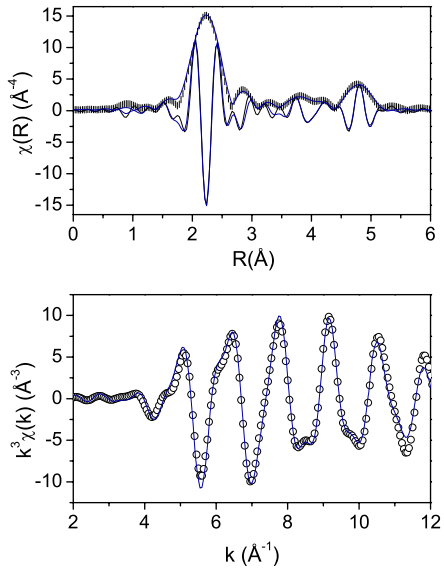

Figure 7. Magnitude and real component of FT of EXAFS spectra in R space and real component of FT in the back transformed k space for the Mn K-edge in $Ni_{50}Mn_{35}Sn_{15}$ obtained at low temperature. The solid line represents the fit to the data.

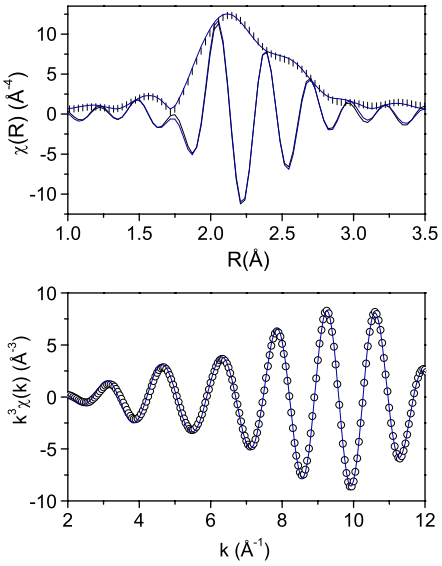

Figure 8. Magnitude and real component of FT of EXAFS spectra in R space and real component of FT in the back transformed k space for Ni K-edge in $Ni_{50}Mn_{35}Sn_{15}$ obtained at low temperature. Fit to the data is shown as a solid line.

Heusler intermetallics, having generic formula X_2YZ. The stoichiometric Ni_2MnSn is a ferromagnet with $T_C \sim 360$ K but does not undergo any martensitic transformation [11]. The exchange interactions in such Heusler alloys is mainly due to the indirect RKKY interaction between Mn atoms mediated by the conduction electrons of the system [18]. As Mn concentration is increased, martensitic phase transformation sets in and magnetism becomes even more complex. The magnetization results reported in the previous section show that $Ni_{50}Mn_{35}Sn_{15}$ orders ferromagnetically at $T_C = 319$ K and undergoes a martensitic transformation ~200 K.

The important result of the EXAFS study is that the local distortions exist in the crystal structure within the cubic framework. These distortions are reflected through a shorter Ni–Mn distance and distinctly different Ni–Sn and Ni–Mn bond lengths. The Ni–Mn distance obtained from EXAFS analysis is the average bond length of Ni–[Y-Mn] and Ni–[Z-Mn]. Since the atomic sizes of Sn and Mn are different, a local distortion can occur when Mn atoms occupy the Sn sites. This can lead to a shorter Ni–[Z-Mn] distance as compared to Ni–[Y-Mn] distance. This distortion in the $L2_1$ structure may be one of the factors that influence the martensitic transformation in $Ni_{50}Mn_{35}Sn_{15}$. A shorter Ni–[Z-Mn] bond implies stronger hybridization of Ni with Z-Mn. The hybridization features between X and Z species of the X_2YZ metallic systems is known to influence the binding mechanism [19]. In the case of $Ni_{50}Mn_{35}Sn_{15}$, the stronger Ni–[Z-Mn] hybridization perhaps results in a redistribution of electrons, causing changes in the DOS at the Fermi level and leading to a martensitic transition. This is further supported by XANES spectroscopy. Figure 9 shows the near-edge structure at Mn and Ni K-edges in austenitic and martensitic phases. It can be clearly seen that, while the Ni edge shifts by ~0.7 eV to higher energy in the martensitic phase, the Mn edge shifts lower by an exactly similar amount. Such shifts in the edge position have been attributed to hybridization effects dominant near the Fermi level, for example in hydrogen incorporated Pd films [20]. Therefore the exactly opposite shifts in Mn and Ni edge positions imply that in the martensitic phase there is a hybridization between Mn(d) and Ni(d) states near the Fermi level.

The martensitic phase change in shape memory alloys is a volume conserving transformation [21]. Therefore the weighted average for each bond distance obtained from EXAFS analysis in the martensitic phase should be nearly equal to that obtained in the austenitic phase. Indeed this is observed for all distances except for Mn–Sn and Mn–Mn bonds that shorten from 2.95 to 2.87 Å. This indicates that the observed modulated low temperature phase is mainly due to the movement of Mn atoms. The movement of Mn atoms implies that there is a redistribution of Ni–[Y-Mn] and Ni–[Z-Mn] bond distances that gives an average Ni–Mn value that is different from that in the cubic phase. Such redistribution results in a scenario wherein the tetrahedral cage of Ni–[Y-Mn] expands, giving room for the Ni–[Z-Mn] tetrahedron to shrink and form stronger hybrid states. This situation is analogous to that observed in $Ni_{2+x}Mn_{1-x}Ga$ alloys [17]. Here, upon undergoing martensitic transition, the Mn atoms occupying the Y site move away from Ni while the Ga atoms that occupy the Z site form stronger bonds with Ni.

Band structure calculations for a X_2MnZ Heusler system [18] have shown that the spin-up 3d states of Mn are fully occupied and hybridized with the d states of the X atoms. Whereas the spin down d states are nearly empty and are almost completely excluded from the Mn site. This results in a localized magnetic moment of Mn. The Z atoms provide electrons to form hybrid states with d electrons of transition metals and through their valence also determine the degree

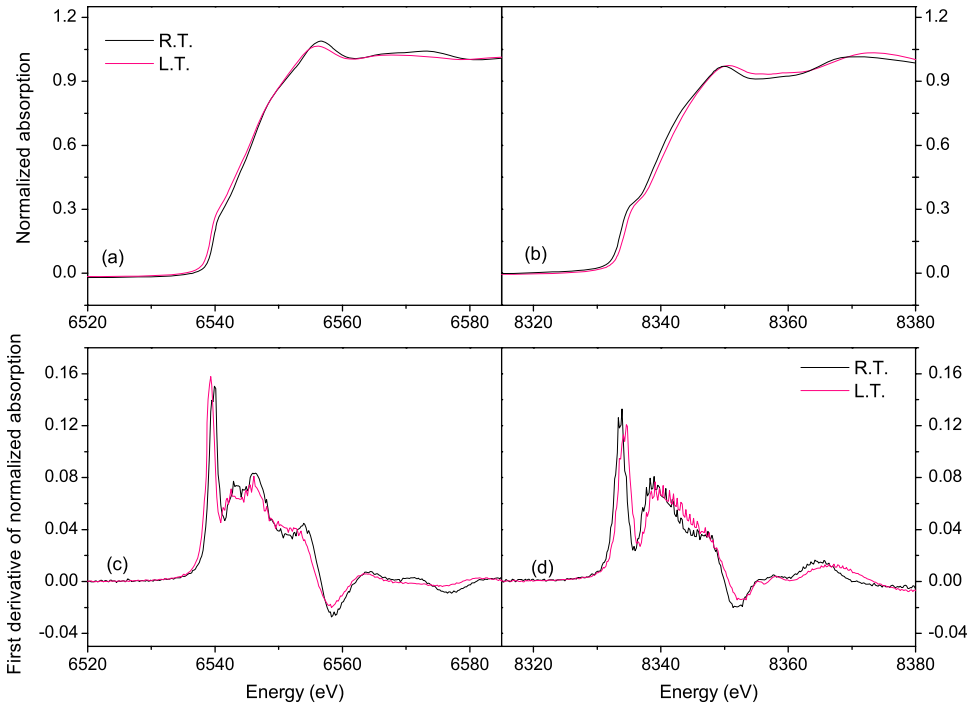

Figure 9. Near edge structure at the Mn K-edge (a) and Ni K-edge (b) in the austenitic and martensitic phases in $Ni_{50}Mn_{35}Sn_{15}$. The first derivative of the near-edge spectra is shown for the Mn K-edge (c) and Ni K-edge (d) at room temperature and low temperature.

of occupation of hybrid orbitals. In the case of Ni_2MnGa, Zayak *et al* [19] have shown that due to the presence of the large local magnetic moment of Mn, spin down 3d electrons of Ni do not find symmetry allowed d states of Mn to hybridize with. This results in a electrostatic like repulsion between Mn and Ni atoms and leads to a attractive interaction between spin down 3d electrons of Ni and 4p electrons of Ga. Such pd hybridization gives rise to a peak in the density of states that is believed to be responsible for martensitic transformation in this alloy. In $Ni_{50}Mn_{35}Sn_{15}$, our EXAFS study gives lower average Ni–Mn distances as compared to the calculated ones in the austenitic as well as martensitic phase. Further, the XRD profile for $Ni_{50}Mn_{35}Sn_{15}$ indicates the room temperature austenitic phase to be highly ordered in the $L2_1$ structure. This observation implies that the lower average Ni–Mn distance seen from EXAFS results from shorter Ni–[Z-Mn] bonds. In other words, the Z-Mn is closer to Ni than Y-Mn and Sn atoms. This results in a Ni-d and Z-Mn-d hybridization that leads to Jahn–Teller distortion affecting the density of states at E_F and driving the system to a martensitic transition.

5. Conclusions

In conclusion, the analysis of the EXAFS measurements at Ni and Mn K-edges in the austenitic and martensitic phases provides a possible explanation for the occurrence of martensitic transition in $Ni_{50}Mn_{35}Sn_{15}$. The $M(T)$ data confirm the temperatures of structural and magnetic phase transformations. The results of the EXAFS analysis reveal a local structural disorder in the cubic phase itself that might be the cause for the system to be unstable towards structural transition. Mn atoms are found to move with maximum amplitude from their crystallographic position when forming a modulated martensitic structure. The unequal Ni–Mn bond lengths that result from the presence of excess Mn in the system show that it is the *dd* hybridization between Ni and Z-Mn that is responsible for martensitic transformation in $Ni_{50}Mn_{35}Sn_{15}$.

Acknowledgments

The authors gratefully acknowledge financial assistance from the Department of Science and Technology, New Delhi, India and ICTP-Elettra, Trieste, Italy for the proposal 2005743. Thanks are also due to Dr Luca Olivi for help in EXAFS measurements. PAB would like to thank the Council for Scientific and Industrial Research, New Delhi for financial assistance.

References

[1] Vasil'ev A N, Buchel'nikov V D, Takagi T, Kholvailo V V and Estrin E I 2003 *Phys.—Usp.* **46** 559
[2] Soderberg O, Ge Y, Sozinov A, Hannula S-P and Lindroos V K 2005 *Smart Mater. Struct.* **14** S223
[3] Entel P, Buchelnikov V D, Khovailo V V, Zayak A T, Adeagdo W A, Gruner M E, Herper H C and Wassermann E F 2006 *J. Phys. D: Appl. Phys.* **39** 865
[4] Webster P J, Ziebeck K R A, Town S L and Peak M S 1984 *Phil. Mag.* **49** 295
[5] Pareti L, Solzi M, Albertini F and Paoluzi A 2003 *Eur. Phys. J.* B **32** 303
[6] Sutou Y, Imano Y, Koeda N, Omori T, Kainuma R, Ishida K and Oikawa K 2004 *Appl. Phys. Lett.* **85** 4358
[7] Krenke T, Duman E, Acet M, Wassermann E, Moya X, Manosa L and Planes A 2005 *Nat. Mater.* **4** 450

[8] Brown P J, Grandy A P, Ishida K, Kainuma R, Kanomata T, Neumann K-U, Oikawa K, Ouladdiaf B and Ziebeck K R A 2006 *J. Phys.: Condens. Matter* **18** 2249
[9] Krenke T, Acet M, Wassermann E F, Moya X, Manosa L and Planes A 2005 *Phys. Rev.* B **72** 014412
[10] Koyama K, Watanabe K, Kanomata T, Kainuma R, Oikawa K and Ishida K 2006 *Appl. Phys. Lett.* **88** 132505
[11] Webster P J and Ziebeck K R A 1988 *Alloys and Compounds of d-Elements with Main Group Elements Part 2* (*Landolt-Börnstein, New Series,* Group III, vol 19/c) ed H R J Wijn (Berlin: Springer)
[12] Newville M 2001 *J. Synchrotron Radiat.* **8** 322
[13] Ravel B and Newville M 2005 *J. Synchrotron Radiat.* **12** 537
[14] Ravel B 2001 *J. Synchrotron Radiat.* **8** 314
[15] Zabinsky S I, Rehr J J, Ankudinov A, Albers R C and Eller M J 1995 *Phys. Rev.* B **52** 2995
[16] Koyama K, Okada H, Watanabe K, Kanomata T, Kainuma R, Ito W, Oikawa K and Ishida K 2006 *Appl. Phys. Lett.* **89** 182510
[17] Bhobe P A, Priolkar K R and Sarode P R 2006 *Phys. Rev.* B **74** 224425
[18] Kübler J, Williams A R and Sommers C B 1983 *Phys. Rev.* B **28** 1745
[19] Zayak A T, Entel P, Rabe K M, Adeagbo W A and Acet M 2005 *Phys. Rev.* B **72** 054113
[20] Ruckman M W, Reisfeld G, Jisrawi N M, Weinert M, Strongin M, Wiesmann H, Croft M, Sahiner A, Sills D and Ansari P 1998 *Phys. Rev.* B **57** 3881
[21] Bhattacharya K 2003 *Microstructure of Martensite: Why It Forms and How It Gives Rise to Shape Memory Effect* (Oxford: Oxford University Press)